OPEN ACCESS
JOURNAL OF ADVANCED DIELECTRICS
Vol. 14, No. 3 (2024) 2440009 (8 pages)

DOI: 10.1142/S2010135X24400095

Multifunctional BNT-based ferroelectric ceramics with large electrostrain and strong photoluminescence properties

Di Wang, Jiaqi Zhao, Yue Li, Chengshuo Zhang, Luchang Yu, Yaqi Zhang, Xiaohua Yang, Jigong Hao *,‡ and Wei Li †,‡
Laboratory of Sensitive Materials and Devices
Shandong Department of Education, School of Materials Science and Engineering
Liaocheng University, Liaocheng 252059, P. R. China
*haojigong@lcu.edu.cn
†liwei_727@163.com

Received 28 December 2023; Revised 15 March 2024; Accepted 21 March 2024; Published 30 April 2024

The development of multifunctional materials with optical and electrical properties has become a research hotspot in recent years. In this work, multifunctional $0.935(Bi_{0.5}Na_{0.5})TiO_3$–$0.065BaTiO_3$ (BNT–BT)-based ferroelectric ceramics doped with small amounts of $CaMAlO_4$ (M = Dy, Ho) were prepared, and the effect of $CaMAlO_4$ on the electrostrain and photoluminescence properties of the ceramics was studied. The results showed that the $CaMAlO_4$ addition weakened the ferroelectric properties of the BNT–BT matrix, and promoted the improvement of the electrostrain performance. For samples doped with 1.5 mol% $CaMAlO_4$, the unipolar strain S_{uni} reached the largest values, which were 0.33% (M = Dy) and 0.38% (M = Ho) under an electric field of 70 kV/cm, corresponding to a large signal d^*_{33} (S_{max}/E_{max}) of 471 pm/V (M = Dy) and 543 pm/V (M = Ho), respectively. In addition, due to the existing Dy^{3+} and Ho^{3+} luminescent ions, the modified samples exhibited excellent photoluminescence performance, which exhibited bright yellow emission (M = Dy) and green emission (M = Ho) under the blue excitation. Due to their multifunctional features, these materials have potential applications as "on-off" actuators, optical-electro integration and coupling devices.

Keywords: Ferroelectric ceramics; perovskite; electrostrain; photoluminescence.

1. Introduction

Piezoelectric ceramics have been widely used in commercial applications as sensors, actuators and transducers. The commercial piezoelectric ceramics currently used in applications are mainly lead-based ceramics represented by $Pb(Zr, Ti)O_3$.[1,2] However, the toxic lead element pollutes the environment and harms human health. Therefore, with the requirements of sustainable development and national policies and regulations, there is a great need to develop lead-free piezoelectric candidates.[3,4]

Among various kinds of lead-free piezoelectric ceramic systems, $(Bi_{0.5}Na_{0.5})TiO_3$ (BNT) is considered a promising piezoelectric material,[4–6] which has a typical perovskite structure (ABO_3) and shows strong ferroelectricity. By adding the other components [$BaTiO_3$, $(Bi_{0.5}K_{0.5})TiO_3$, etc.] and forming the morphotropic phase boundary (MPB) in the new solid solution, enhanced piezoelectric and electrostrain performance can be achieved.[5] Over the last two decades, many researchers have carried out in-depth studies on the high electrostrain performance of BNT-based ceramics and achieved a series of research results.[7–11] Deng *et al.*[8] reported enhanced strain properties in La^{3+}-doped BNT-based ceramics, which achieved a high strain response of 0.40–0.42% under 60–70 kV/cm, yielding large signal d^*_{33} of 600–630 pm/V. Shi *et al.*[9] added two MPB modifiers $[Li_{0.06}(K_{0.5}Na_{0.5})_{0.94}]NbO_3$ and $(Ba_{0.85}Ca_{0.15})(Ti_{0.9}Zr_{0.1})O_3$ into the BNT ceramic, and achieved a high strain of 0.50% with a large signal d^*_{33} of 625 pm/V. Yin *et al.*[10] reported a high unipolar strain response (S = 0.53–0.56%, d^*_{33} = 883–933 pm/V, at 60 kV/cm) in $\{[Bi_{0.5}(Na_{0.82-x}K_{0.18}Li_x)_{0.5}]_{(1-y)}$-$Sr_y\}(Ti_{1-z}Ta_z)O_3$ ceramics and studied the origin of the giant strain. Very recently, Jia *et al.*[11] reported a strategy to obtain giant electrostrain by manipulating defect dipoles in $(Bi_{0.5}Na_{0.5})TiO_3$–$BaTiO_3$-based ceramics, and obtained a high electrostrain of 1.68% at 85 kV/cm, corresponding to a large signal d^*_{33} as high as 1965 pm/V. Studies have shown that the electrostrain performance of BNT-based ceramics mainly comes from the reversible phase transition of ferroelectric phase and relaxor phase under the application of electric field.[5,7] To achieve high electrostrain performance of BNT-based materials, the most commonly used approach is chemical doping modification of BNT matrix near MPB.[7,12] Thus, the ferroelectric long-range order of the matrix is destroyed, resulting in the formation of a relaxor state and achieving a reversible transition of ferroelectric-relaxor state under the electric field. As a result, it generates the field-induced large strain response.[13]

‡Corresponding authors.

On the other hand, developing multifunctional characteristics of piezoelectric materials has stimulated increased scientific interest in recent years. As recognized luminescent active ions, rare earth (RE^{3+}) ions have good luminous properties due to their abundant electronic energy levels. Therefore, through doping RE^{3+} into piezoelectric ceramics, materials exhibit rich fluorescence emission, which is of great value for the development of multifunctional piezoelectric materials.[14–23] For BNT-based materials, the doping of RE^{3+} ions not only acts as luminescent-activated ions, but also plays a "disturbing effect" on the long-range ferroelectric ordering and optimizes the electrostrain of BNT-based ceramics.[19–23] Kuang *et al.*[19] used Pr^{3+} as the dopant ions to active the photoluminescent properties of $0.94(Bi_{0.5}Na_{0.5})$-TiO_3–$0.06BaTiO_3$ ceramics. Strong red emission and high electrostrain of 0.58% (80 kV/cm) were simultaneously obtained in the Pr^{3+}-modified sample. Yao *et al.*[21] obtained large strain response and excellent photoluminescence properties in Pr^{3+}-modified $0.93(Bi_{0.5}Na_{0.5})TiO_3$–$0.07BaTiO_3$ ceramics and found the photoluminescence-enhancement effect induced by the *in situ* electric field. Zhao *et al.*[22] prepared the Er^{3+}-modified $0.93Bi_{0.5}Na_{0.5}TiO_3$–$0.07BaTiO_3$ multifunctional ceramics with improved electric-field-induced strain and bright green light emission properties.

In this work, $CaMAlO_4$ (M = Dy, Ho) with a K_2NiF_4-type structure[24] was selected as the dopant. When forming a solid solution with BNT-based ceramics, Ca^{2+} and M^{3+} (M = Dy, Ho) will occupy the A-site of the perovskite structure, and Al^{3+} will occupy the B-site of the perovskite structure considering their ion radius, which is conducive to enhancing relaxation of the BNT-based ceramics and improving the strain response. Moreover, relying on the luminescence effect of rear earth ions (Dy^{3+}, Ho^{3+}), the modified BNT-based ceramics are expected to exhibit luminescence properties. Based on the above, we prepared $CaMAlO_4$-modified $0.935(Bi_{0.5}Na_{0.5})TiO_3$-$0.065BaTiO_3$ ceramics, and systematically studied the effect of $CaMAlO_4$ on the phase structure, electrostrain and photoluminescence properties of BNT-based ferroelectric ceramics.

2. Experimental

$(1-x)[0.935(Bi_{0.5}Na_{0.5})TiO_3$–$0.065BaTiO_3]$–$xCaMAlO_4$ (abbreviated as BNT–BT–xCMA; M = Dy, Ho; $x = 0.003$–0.018) lead-free ferroelectric ceramics were prepared by the traditional solid-state reaction method. The raw materials selected were $BaCO_3$ (99%), Na_2CO_3 (99.8%), Bi_2O_3 (99.5%), TiO_2 (99.5%), $CaCO_3$ (99%), Dy_2O_3 (99.9%), Ho_2O_3 (99.9%) and Al_2O_3 (99.99%). The raw materials were weighed and then ball-milled in the planetary ball mill using ZrO_2 grinding balls and absolute ethanol as a grinding medium. The raw materials after ball milling were dried in the oven for about 4 h. The dried mixture was pressed into a disc and calcined at 850°C for 4 h to synthesize the precursor powder. After the powders were subjected to the ball milling again, an appropriate amount of 10 wt.% polyvinyl alcohol (PVA) adhesive was added for granulation. The powder was pressed into discs and then heated in the furnace to remove the binder. Finally, samples were sintered at 1120°C for 2 h to obtain the ceramics and the heating rate was 3°C/min. For electrical properties' measurements, silver paste was coated on the surface of the ceramic and fired at 650°C to form electrodes.

The phase structure of ceramics was identified by an X-ray diffractometer (XRD, D8 advance, Bruker, Germany). The temperature dependence of dielectric properties was measured by the temperature dielectric test system (HCT-1821, Tongguo Technology, China). The ferroelectric and strain properties of the samples were measured by a ferroelectric analyzer (TF Analyzer 2000, aix-ACCT, Germany) connected with SP-S120 laser interferometer (SIOS, SIOS Meβtechnik GmbH, Germany). The photoluminescence (PL) and photoluminescence excitation (PLE) spectra of the samples were measured using fluorescence spectrometers (FLS920, Edinburgh Instruments, UK).

3. Results and Discussion

3.1. *Phase structure*

Figures 1(a) and 1(b) show the XRD patterns of BNT–BT–xCMA (M = Dy, Ho) ceramics. It can be seen from the figure that all samples form a single perovskite structure, which indicates that CMA has formed a uniform solid solution with the BNT–BT matrix. The right picture shows the enlarged XRD patterns in the 2θ range of 42–50°. According to the literature reports, BNT–BT ceramic has a coexistence structure of rhombohedral (R)–tetragonal (T) coexisting phases, evident by the peak splitting at around $2\theta \sim 46°$ of (002)/(200) reflections.[25] With the addition of CMA, the (002)/(200) diffraction splitting peaks gradually evolve into a single (200) peak. When $x = 0.012$, the (002) peak has completely disappeared, indicating that the addition of CMA induces the phase transition from a R–T coexisting structure to a pseudo-cubic (P_c) phase structure.[26] Improvement of the material's structural symmetry is helpful for the destruction of ferroelectric long-range ordering and the improvement of electrostrain in BNT-based ceramics.

3.2. *Dielectric properties*

Figure 2 shows the temperature dependence of the dielectric constant (ε_r) of BNT–BT–xCMA ceramics recorded at 10 kHz. It can be clearly observed from the figure that the sample has two dielectric peaks above room temperature. According to the previous literature report, the dielectric peak T_m at the maximum dielectric constant at high temperature represents the transition from the tetragonal "anti-ferroelectric" phase to the cubic paraelectric phase, and the relatively weak dielectric peak T_s at low temperature represents the

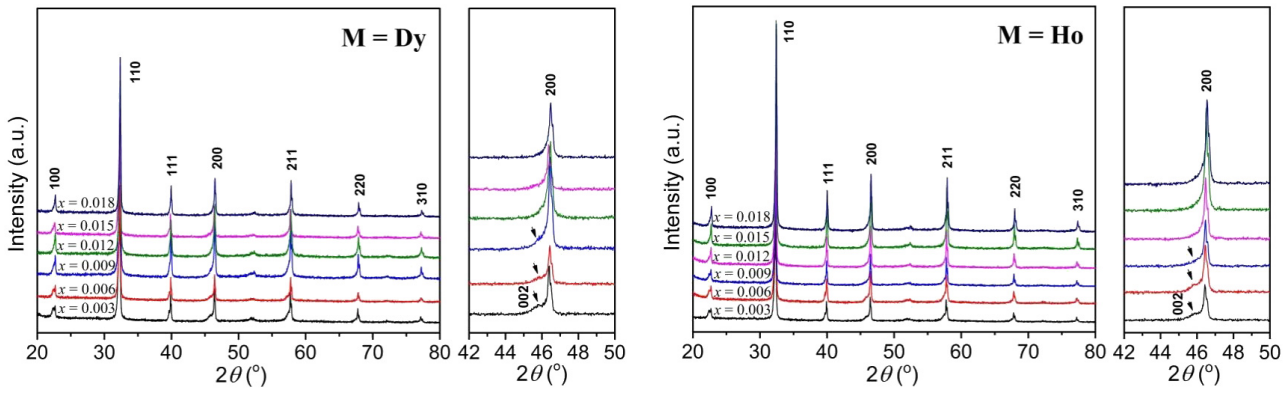

(a) (b)

Fig. 1. XRD patterns of BNT–BT–xCMA ceramics: (a) M = Dy, (b) M = Ho.

transition from the rhombohedral ferroelectric phase to the tetragonal "anti-ferroelectric" phase of the material.[27] In recent years, it has been proposed that the dielectric peak of T_m is a relaxor transition from the rhombohedral polar nanoregions to the tetragonal nanoregions, while the dielectric anomaly at T_s is caused by the thermal evolutions of the discrete polar nanoregions.[28] With the increased content of CMA, the dielectric constant of the sample in the whole temperature range gradually decreases. The ε_r–T curve between T_s and T_m becomes flattening, indicating that the dielectric relaxor of the sample is enhanced. This can be related to the enhanced structural symmetry of the modified samples.

3.3. *Ferroelectric and electrostrain properties*

Figures 3(a)–3(f) show the P–E loops and unipolar/bipolar strain curves of BNT–BT–xCMA ceramics recorded at room temperature and 10 Hz. At low content of CMA ($x = 0.003$), the materials exhibit saturation hysteresis loops and "butterfly" shaped strain curves with obvious negative electrostrain S_{neg} ($S_{neg} \sim 0.15\%$), typical for normal ferroelectrics.[29] Meanwhile, the unipolar electrostrain has a linear relationship with the electric field, and the unipolar strain value is low ($S_{uni} \sim 0.10\%$). With the increase of CMA content, P–E loops become pinched and the remanent polarization P_r decreases significantly. This indicates that the addition of CMA destroys the ferroelectric long-range ordering of the BNT–BT.[23] The weakened ferroelectric performance induced by the CMA doping can be linked to the increased symmetry of crystal structure, as noted that the addition of CMA induces the phase transition from a R–T coexisting structure to a pseudo-cubic (P_c) phase structure. The bipolar strain curves of the sample present a "sprout" shape and S_{neg} disappears. The unipolar strain of the material is significantly increased ($S_{uni} > 0.33\%$). At $x = 0.015$, the unipolar strains S_{uni} of the sample reach the maximum value, which are 0.33% (M = Dy) and 0.38% (M = Ho) under 70 kV/cm. The corresponding large signal piezoelectric constants d^*_{33} ($d^*_{33} = S_{max}/E_{max}$) are 471 pm/V (M = Dy) and 543 pm/V (M = Ho), respectively, as shown in Figs. 3(g) and 3(h).

Figures 4(a)–4(f) show the P–E loops and unipolar/bipolar strain curves of BNT–BT–xCMA (M = Ho, $x = 0.003$,

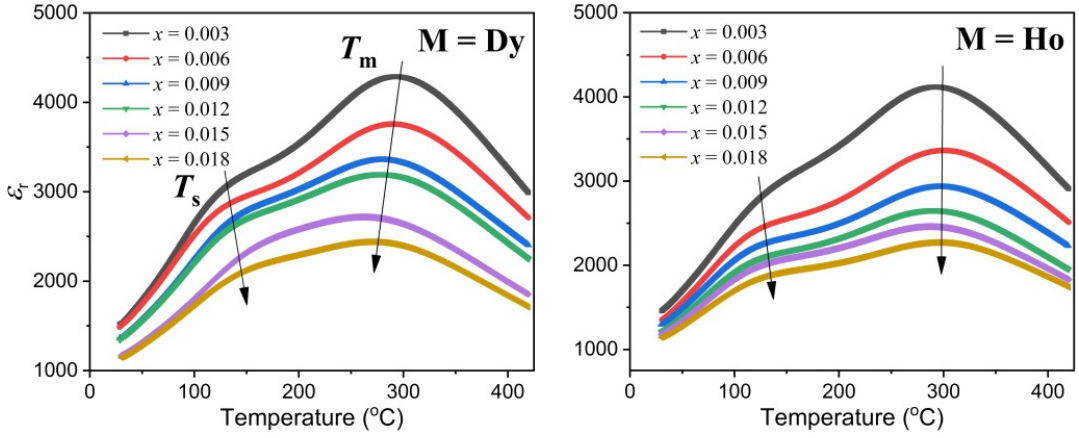

(a) (b)

Fig. 2. Temperature dependence of the dielectric constant of BNT–BT–xCMA ceramics recorded at 10 kHz: (a) M = Dy, (b) M = Ho.

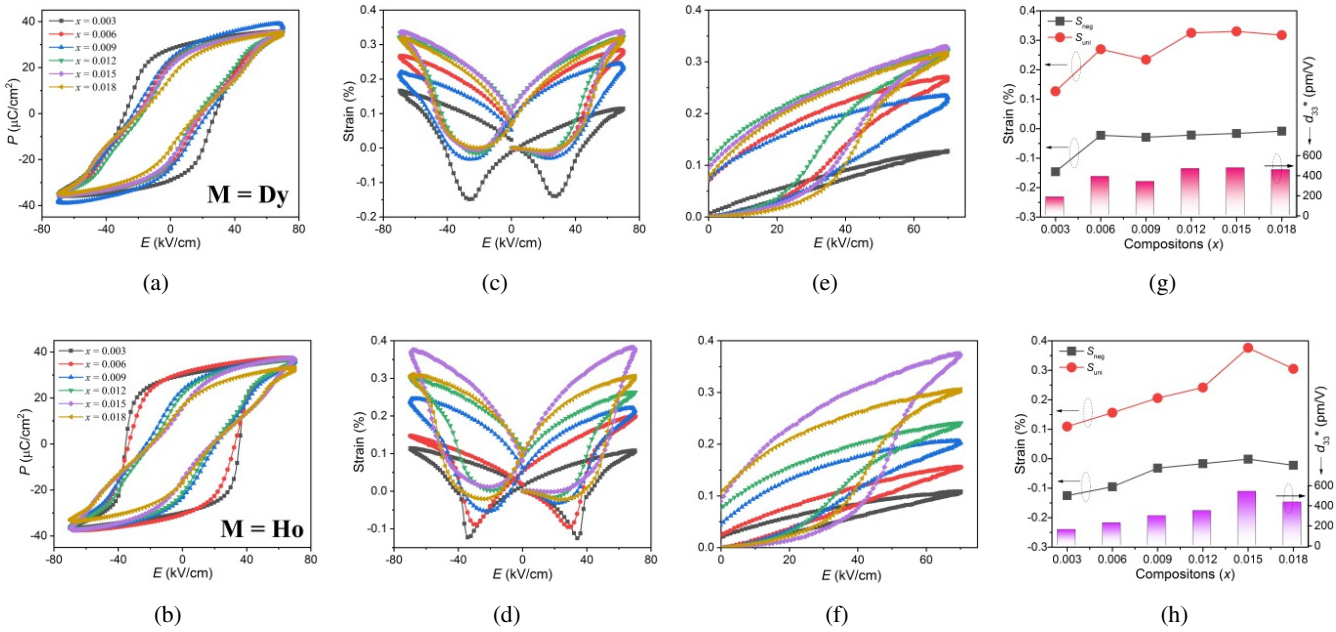

Fig. 3. (a), (b) *P–E* hysteresis loops and (c)–(f) bipolar/unipolar strain curves of BNT–BT–*x*CMA (M = Dy, Ho) ceramics measured at 10 Hz. (g), (h) Compositional dependence of unipolar strain (S_{uni}), negative strain (S_{neg}) and normalized strain d^*_{33} values for BNT–BT–*x*CMA (M = Dy, Ho) ceramics.

0.015) ceramics measured at different temperatures at 10 Hz. For the $x = 0.003$ sample, the *P–E* loops gradually change from a rectangle shape to a pinched shape with the increase of temperature, and the remanent polarization P_r decreases significantly. At the same time, the bipolar *S–E* curves gradually change from "butterfly" shape to "sprout" shape, and S_{neg} gradually disappears. These changes indicate that this composition undergoes a phase transition from a ferroelectric state to a relaxor state as temperature increases,[23] which significantly improves the strain response. As shown in Fig. 4(g), when the temperature is 100°C, the S_{uni} of the sample reaches the maximum value of 0.35% (70 kV/cm), corresponding to the d^*_{33} of 500 pm/V. For the $x = 0.015$ sample, it shows a weak polar state at initial temperature. When the electric field is applied, the weak polar state reversibly transforms to the ferroelectric state, yielding a large strain value of 0.35%. With the increase in temperature, the shapes of *P–E* loops and unipolar/bipolar strain curves do not change significantly. The S_{uni} shows a slight increase with the temperature and reaches the maximum value of 0.38% (70 kV/cm) at 35°C, corresponding to the d^*_{33} of 543 pm/V. After that, the S_{uni} decreases gradually with temperature. In the temperature range of 20–100°C, the changing rate of strain value is relatively small, and its decline degree is only about 23%, suggesting relatively good temperature stability.

3.4. *Photoluminescence properties*

In this study, the CMA addition not only improves the electrostrain properties of BNT–BT ceramics, but also renders the materials to exhibit strong photoluminescence properties due to the presence of rare earth luminescent ions in the CMA composition. Figure 5(a) shows the PLE and PL spectra of BNT–BT–*x*CMA (M = Dy, $x = 0.003$) ceramics. The PLE spectrum shows four excitation peaks in the range of 300–500 nm, which locate at the wavelengths of 390, 429, 453 and 474 nm, corresponding to the energy level transitions from the ground state $^6H_{15/2}$ to the excited states $^4K_{17/2}$, $^4G_{11/2}$, $^4I_{15/2}$ and $^4F_{9/2}$, respectively.[30–32] Under the excitation of blue light at 453 nm wavelength, the sample produce three emission peaks in the range of 480–700 nm, which locate at the wavelengths of 482, 576 and 665 nm, respectively. These emission peaks correspond to the weak blue-light emission of $^4F_{9/2} \rightarrow {}^6H_{15/2}$, strong yellow light emission of $^4F_{9/2} \rightarrow {}^6H_{13/2}$ and weak red-light emission of $^4F_{9/2} \rightarrow {}^6H_{11/2}$, respectively.[31] This result corresponds to the CIE chromaticity coordinate position ($x = 0.3871$, $y = 0.4915$), which is the yellow region, as shown in Fig. 5(c). Figure 5(b) shows the PL spectra of BNT–BT–*x*CMA (M = Dy) ceramics. With the increase of CMA (M = Dy) doping content, the content of luminescence centers Dy^{3+} gradually increases. Accordingly, it promotes the increase of PL intensity, which reaches the maximum value at $x = 0.012$. When $x > 0.012$, the PL intensity gradually decreases due to the concentration-quenching effect.[32]

Figure 5(d) shows the PLE and PL spectra of BNT–BT–*x*CMA (M = Ho, $x = 0.003$) ceramics. The PLE spectrum has four excitation peaks in the range of 300–500 nm, which locate at the wavelengths of 419, 454, 469 and 486 nm, corresponding to the energy level transitions from the ground state $^5I_8$ to the excited states $^5G_5$, $^5G_6$, $^5K_8 + {}^5F_2$ and $^5F_3$, respectively.[33–35] Under the excitation of blue light at 454 nm

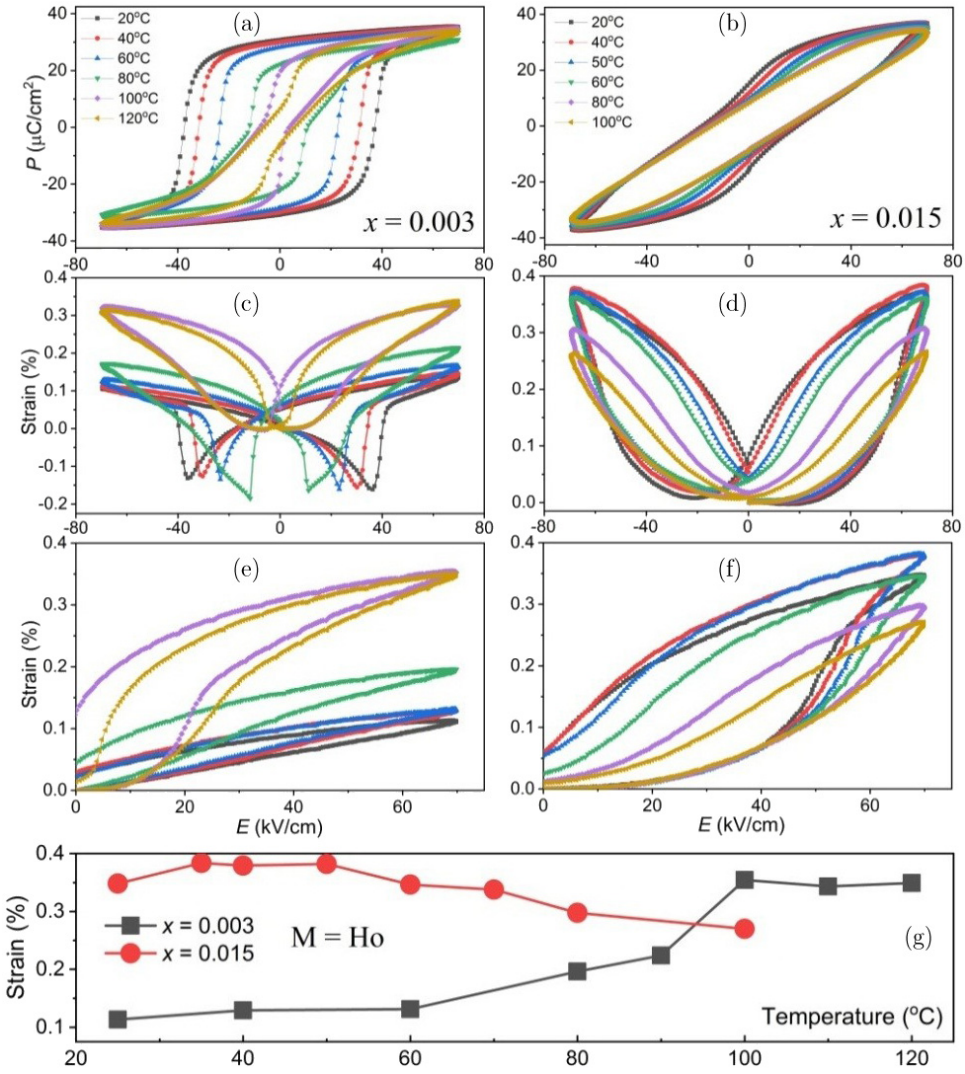

Fig. 4. Temperature-dependent (a), (b) *P*–*E* hysteresis loops and (c)–(f) bipolar/unipolar strain curves for BNT–BT–*x*CMA (M = Ho, $x = 0.003$, 0.015) ceramics at 10 Hz. (g) Variations of S_{uni} values with temperature, for BNT–BT–*x*CMA (M = Ho, $x = 0.003$, 0.015) ceramics.

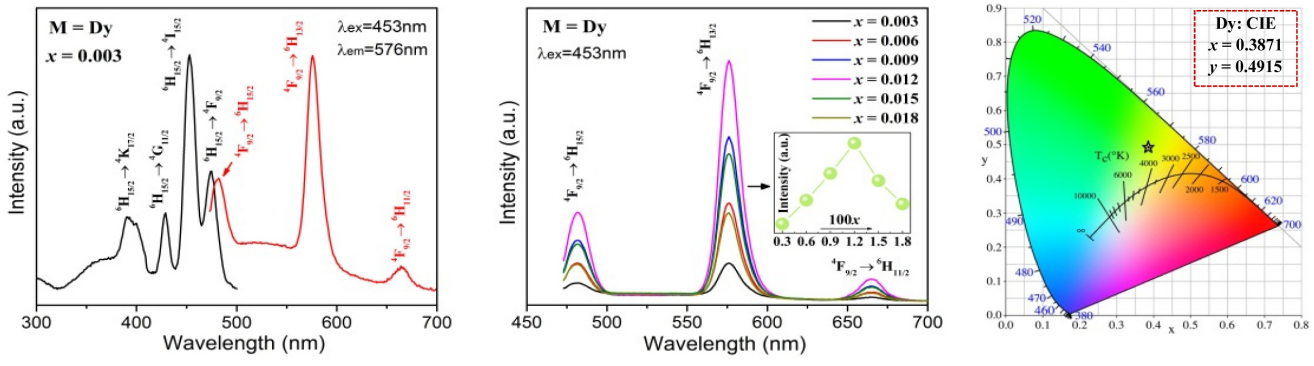

Fig. 5. PLE, PL spectra and the calculated CIE chromaticity coordinates of the samples based on the emission spectra for BNT–BT–*x*CMA ($x = 0.003$) ceramics: (a)–(c) M = Dy, (d)–(f) M = Ho.

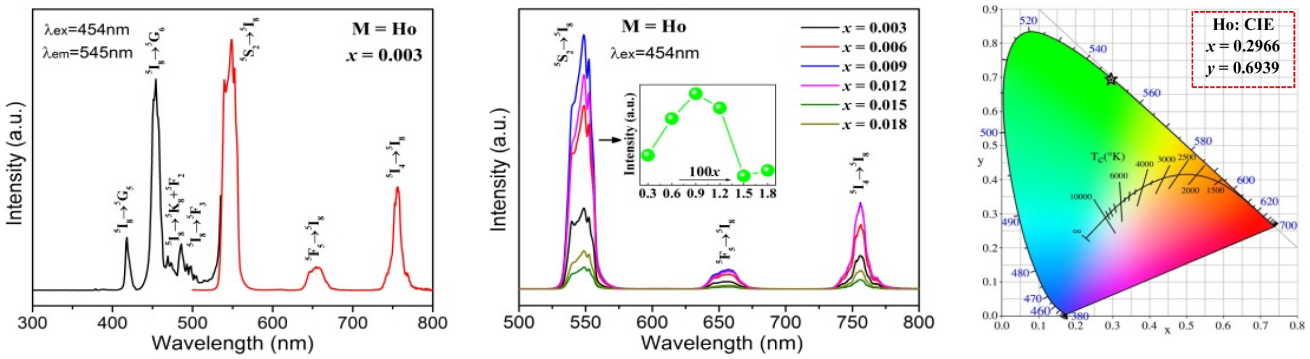

(d) (e) (f)

Fig. 5. (*Continued*)

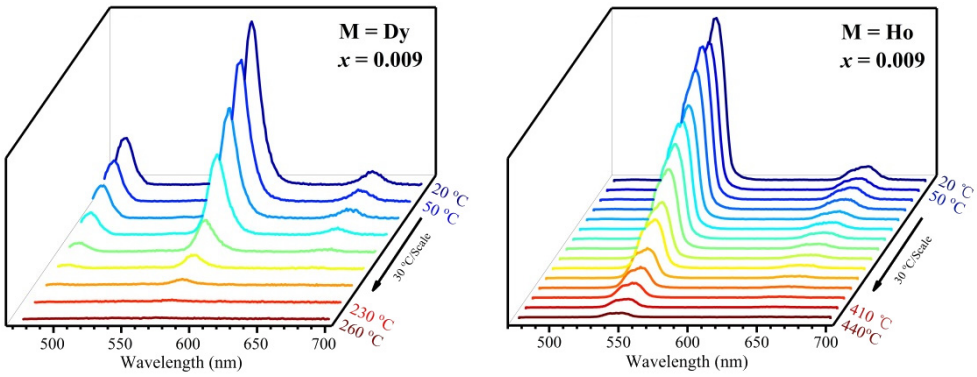

(a) (b)

Fig. 6. PL spectra recorded at different temperatures for BNT–BT–xCMA ($x = 0.009$) ceramics: (a) M = Dy, (b) M = Ho.

wavelength, the sample produces three emission peaks in the range of 500–800 nm, locating at 549, 654 and 756 nm wavelengths and corresponding to the strong green emission of $^5S_2 \rightarrow {}^5I_8$, the weak red emission of $^5F_5 \rightarrow {}^5I_8$ and $^5I_4 \rightarrow {}^5I_8$, respectively.[33] This result corresponds to the CIE chromaticity coordinate position ($x = 0.2966$, $y = 0.6939$), which is the green region, as shown in Fig. 5(f). Figure 5(e) shows the PL spectra of BNT–BT–xCMA (M = Ho) ceramics. With the increase of xCMA (M = Ho) doping amount, the PL intensity increases and reaches the maximum value at $x = 0.009$. When $x > 0.009$, the emission peak intensity also shows a decreasing trend due to the concentration-quenching effect.[35]

Figures 6(a) and 6(b) show the variations of PL spectra with temperature of BNT–BT–xCMA (M = Dy, Ho, $x = 0.009$) ceramics. At low temperatures, the PL spectra peak is stronger. With the increase in temperature, the nonradiative transition probability of the electron in the active ion increases, which causes the temperature-quenching effect.[36] Therefore, the relative intensity of spectral peaks greatly reduces. Compared with the two compositions, we found that the doped sample with CMA (M = Ho) has better high-temperature luminescence performance. When the temperature rises above 400°C, the temperature quenching effect starts to become apparent.

4. Conclusions

BNT–BT–xCMA multifunctional ceramics with large electrostrain and strong photoluminescence properties were prepared. By introducing the $CaMAlO_4$ (M = Dy, Ho) into BNT–BT, the ferroelectric long-range order of the ceramics was disrupted, yielding enhanced relaxor behavior and the improvement of the electrostrain performance. When $x = 0.015$, the unipolar strains S_{uni} of the samples reached 0.33% (M = Dy) and 0.38% (M = Ho) under 70 kV/cm, corresponding to the large signal d^*_{33} of 471 pm/V (M = Dy) and 543 pm/V (M = Ho), respectively. In addition, due to the addition of rare earth ions in the CMA, the materials had excellent photoluminescence properties. Under blue excitation, there were significant yellow emission (M = Dy) and green emission (M = Ho). The materials have application potential in the fields of optical-electro integration and coupling devices.

Acknowledgments

This work was supported by the Natural Science Foundation of Shandong Province, China (Nos. ZR2020ME033 and ZR2020ME031). Research Foundation of the Liaocheng University (No. 318011906). Shandong College Students' Innovation and Entrepreneurship Training Program (No. S202210447017), the Undergraduate Training Programs for Innovation and Entrepreneurship of the Liaocheng University (No. cxcy2022022). Di Wang and Jiaqi Zhao contributed equally to this work.

ORCID

Jigong Hao https://orcid.org/0000-0001-6584-2311
Wei Li https://orcid.org/0000-0002-0619-1042

References

[1]H. W. Shi, F. Li, X. L. Yang, M. S. Long, L. Shan, C. C. Wang and J. W. Zhai, High depolarization temperature and superior piezoelectric performance with complex structural evolution in $BiFeO_3$-$PbTiO_3$-$(Sr_{0.7}Bi_{0.2}\square_{0.1})TiO_3$ systems, *J. Materiomics* **8**, 1260 (2022).

[2]Y. X. Luo, T. Pu, S. B. Fan, H. Liu and J. G. Zhu, Enhanced piezoelectric properties in low-temperature sintering PZN-PZT ceramics by adjusting Zr/Ti ratio, *J. Adv. Dielectr.* **12**, 2250001 (2022).

[3]W. Feng, B. C. Luo, S. S. Bian, E. K. Tian, Z. L. Zhang, A. Kursumovic, J. L. MacManus-Driscoll, X. H. Wang and L. T. Li, Heterostrain-enabled ultrahigh electrostrain in lead-free piezoelectric, *Nat. Commun.* **13**, 5086 (2022).

[4]X. Liu, J. Wang, F. Zhu, Y. Li, W. Tian, W. Wang, R. Guo, L. Liu and J. Shi, Surface oxygen vacancy engineering in weak Bi-O bonded ferroelectric bismuth sodium titanate for boosting photocatalytic CO_2 reduction reaction, *J. Mater. Chem. A* (2024), in press, doi: 10.1039/D4TA01030B.

[5]T. Y. Li, C. Liu, P. Shi, X. Liu, R. R. Kang, C. B. Long, M. Wu, S. D. Cheng, S. B. Mi, Y. H. Xia, L. L. Li, D. Wang and X. J. Lou, High-performance strain of lead-free relaxor-ferroelectric piezoceramics by the morphotropic phase boundary modification, *Adv. Funct. Mater.* **32**, 2202307 (2022).

[6]B. R. Moya, A. C. Silva, A. Peláiz-Barranco and J. D. S. Guerra, Structural, microstructural and dielectric characterizations of $(Bi_{0.5}Na_{0.5})TiO_3$ based lead-free ferroelectric ceramics, *J. Adv. Dielectr.* **11**, 2140006 (2021).

[7]J. G. Hao, W. Li, J. W. Zhai and H. Chen, Progress in high-strain perovskite piezoelectric ceramics, *Mater. Sci. Eng. R Rep.* **135**, 1 (2019).

[8]A. P. Deng and J. G. Wu, Enhanced strain and electrostrictive properties in lead-free BNT-based ceramics *via* rare earth doping, *J. Materiomics* **8**, 401 (2022).

[9]P. Shi, T. Y. Li, X. P. Zhu, W. Y. Liu, Q. D. Liu, B. Yang, X. J. Wang, R. R. Kang, S. Yang and X. J. Lou, High strain in $Bi_{0.5}Na_{0.5}TiO_3$-based relaxors by adding two modifiers featuring with morphotropic phase boundary, *Scripta. Mater.* **218**, 114674 (2022).

[10]J. Yin, C. L. Zhao, Y. X. Zhang and J. G. Wu, Ultrahigh strain in site engineering-independent $Bi_{0.5}Na_{0.5}TiO_3$-based relaxor-ferroelectrics, *Acta Mater.* **147**, 70 (2018).

[11]Y. X. Jia, H. Q. Fan, A. Zhang, H. Wang, L. Lei, Q. F. Quan, G. Z. Dong, W. J. Wang and Q. Li, Giant electro-induced strain in lead-free relaxor ferroelectrics via defect engineering, *J. Eur. Ceram. Soc.* **43**, 947 (2023).

[12]P. Y. Fan, K. Liu, W. G. Ma, H. Tan, Q. Zhang, L. Zhang, C. R. Zhou, D. Salamon, S. T. Zhang, Y. J. Zhang, B. Nan and H. B. Zhang, Progress and perspective of high strain NBT-based lead-free piezoceramics and multilayer actuators, *J. Materiomics* **7**, 508 (2021).

[13]L. H. Hou, C. R. Zhou, Q. N. Li, R. Li, C. L. Yuan, J. W. Xu and G. H. Rao, Giant strain with ultra-low hysteresis by tailoring relaxor temperature and PNRs dynamic in BNT-based lead-free piezoelectric ceramics, *Ceram. Int.* **48**, 13125 (2022).

[14]Q. Zhang, L. H. Luo, J. Gong, P. Du, W. P. Li and G. L. Yuan, Photoluminescence, thermoluminescence and reversible photoluminescence modulation of multifunctional optical materials Pr^{3+} doped $K_xNa_{1-x}NbO_3$ ferroelectric ceramics, *J. Eur. Ceram. Soc.* **40**, 3946 (2020).

[15]W. Li, J. G. Hao, P. Fu, J. Du, P. Li, C. C. Hu, Wei Li and Z. X. Yue, Large electrostrictive effect and strong photoluminescence properties in Sm_2O_3-modified lead-free potassium sodium niobate-based piezoelectric ceramics, *J. Materiomics* **6**, 768 (2020).

[16]X. Wu, J. F. Lin, Z. Xu, C. L. Zhao, C. Lin, H. J. Wang, T. F. Lin, X. H. Zheng, B. S. Sa, Q. W. Zhang, K. Wang, Z. M. Sun and J. W. Zhai, Defect management and multi-mode optoelectronic manipulations via photo-thermochromism in smart windows, *Laser Photonics Rev.* **15**, 2100211 (2021).

[17]X. S. Wang, C. N. Xu, H. Yamada, K. Nishikubo and X. G. Zheng, Electro-mechano-optical conversions in Pr^{3+} doped $BaTiO_3$-$CaTiO_3$ ceramics, *Adv. Mater.* **17**, 1254 (2005).

[18]H. L. Sun, M. C. Wong, G. F. Zhou and K. W. Kwok, Tuning electroluminescence performance in Pr-doped piezoelectric bulk ceramics and composites, *J. Materiomics* **7**, 264 (2021).

[19]H. Y. Kuang, X. He, V. Oleg, S. Wu and D. F. Pang, Large electric field-induced strain and excellent photoluminescence properties of Pr-modified $0.94Bi_{0.5}Na_{0.5}TiO_3$-$0.06BaTiO_3$ lead-free ferroelectric ceramics, *Ceram. Int.* **49**, 39576 (2023).

[20]H. L. Sun, X. Wu, D. F. Peng and K. W. Kwok, Room-temperature large and reversible modulation of photoluminescence by in situ electric field in ergodic relaxor ferroelectrics, *ACS Appl. Mater. Interfaces* **9**, 34042 (2017).

[21]Q. R. Yao, F. F. Wang, F. Xu, C. M. Leung, T. Wang, Y. X. Tang, X. Ye, Y. Q. Xie, D. Z. Sun and W. Z. Shi, Electric field-induced giant strain and photoluminescence-enhancement effect in rare-earth modified lead-free piezoelectric ceramics, *ACS Appl. Mater. Interfaces* **7**, 5066 (2015).

[22]S. J. Zhao, Y. Y. Zhang, Q. F. Zhang, H. Li, J. X. Gao, M. Y. Li, W. F. Zhang, J. N. Liu and B. C. Yang, Improved electric-field-induced strain and strong photoluminescence properties in novel Er^{3+}-modified $0.93Bi_{0.5}Na_{0.5}TiO_3$-$0.07BaTiO_3$ multifunctional ceramics, *Ceram. Int.* **48**, 14301 (2022).

[23]Y. Liu, L. L. Liu, P. Li, P. Fu, J. Du, Z. L. Li, H. Y. Li, J. G. Hao, W. Li and H. R. Zeng, Electric field-induced large strain and photoluminescence properties in $SrRECoO_4$ (RE = Pr, Eu, Sm)-modified BNT-based ferroelectric ceramics, *Ceram. Int.* **49**, 8232 (2023).

[24]Y. Xiao, X. M. Chen and X. Q. Liu, Microstructures and microwave dielectric characteristics of $CaRAlO_4$ (R = Nd, Sm, Y) ceramics with tetragonal K_2NiF_4 Structure, *J. Am. Ceram. Soc.* **87**, 2143 (2004).

[25]A. Sasaki, T. Chiba, Y. Mamiya and E. Otsuki, Dielectric and piezoelectric properties of $(Bi_{0.5}Na_{0.5})TiO_3$-$(Bi_{0.5}K_{0.5})TiO_3$ systems, *Jpn. J. Appl. Phys.* **38**, 5564 (1999).

[26]J. G. Hao, B. Shen, J. W. Zhai and H. Chen, Phase transitional behavior and electric field-induced large strain in alkali niobate-modified $Bi_{0.5}(Na_{0.80}K_{0.20})_{0.5}TiO_3$ lead-free piezoceramics, *J. Appl. Phys.* **115**, 034101 (2014).

[27]Y. Hiruma, K. Yoshii, H. Nagata and T. Takenaka, Phase transition temperature and electrical properties of $(Bi_{1/2}Na_{1/2})TiO_3$-$(Bi_{1/2}A_{1/2})TiO_3$ (A = Li and K) lead-free ferroelectric ceramics, *J. Appl. Phys.* **103**, 084121 (2008).

[28]X. Tan, E. Aulbach, W. Jo, T. Granzow, J. Kling, M. Marsilius, H. J. Kleebe and J. Rödel, Effect of uniaxial stress on ferroelectric behavior of $(Bi_{1/2}Na_{1/2})TiO_3$-based lead-free piezoelectric ceramics, *J. Appl. Phys.* **106**, 044107 (2009).

[29]G. Viola, T. Saunders, X. Wei, K. B. Chong, H. Luo, M. J. Reece and H. Yan, Contribution of piezoelectric effect, electrostriction and ferroelectric/ferroelastic switching to strain-electric field response of dielectrics, *J. Adv. Dielectr.* **3**, 1350007 (2013).

[30]M. Sołtys, L. Żur, J. Pisarska and W. A. Pisarski, Excitation and luminescence of Dy^{3+} ions in PbO-P_2O_5-Ga_2O_3 glass system, *J. Rare. Earth* **32**, 213 (2014).

[31]P. P. Pawar, S. R. Munishwar, S. Gautam and R. S. Gedam, Physical, thermal, structural and optical properties of Dy^{3+} doped lithium alumino-borate glasses for bright W-LED, *J. Lumin.* **183**, 79 (2017).

[32]C. L. Ma, Y. Wang, J. Zhang, Y. Hu, Z. Y. Zhai, J. Wu, W. P. Zhou and X. W. Lv, Photoluminescence and optical temperature sensing properties of Dy^{3+}-doped $Na_{0.5}Bi_{0.5}TiO_3$ multifunctional ferroelectric ceramics, *Spectrochim. Acta A Mol. Biomol. Spectrosc.* **254**, 119636 (2021).

[33]T. Wei, Q. J. Zhou, C. Z. Zhao, Y. B. Lin, Y. L. Zou, Y. Li and L. S. Zhang, Strong green light emission in Ho doped $Bi_4Ti_3O_{12}$ ferroelectric ceramics, *Ceram. Int.* **39**, 7211 (2013).

[34]L. Zhou, X. Zou, M. J. Tian, F. Y. Lei, Q. J. Zheng, T. Sun and D. M. Lin, Improved piezoelectric and bright up-conversion photoluminescent properties in Ho-doped $Bi_{0.5}Na_{0.5}TiO_3$-$BaTiO_3$ lead-free ceramics, *J. Mater. Sci. Mater. Electron.* **26**, 6979 (2015).

[35]P. Xiao, Y. Q. Guo, M. J. Tian, Q. J. Zheng, N. Jiang, X. C. Wu, Z. G. Xia and D. M. Lin, Improved ferroelectric/piezoelectric properties and bright green/UC red emission in (Li, Ho)-doped $CaBi_4Ti_4O_{15}$ multifunctional ceramics with excellent temperature stability and superior water-resistance performance, *Dalton Trans.* **44**, 17366 (2015).

[36]S. G. He, F. F. Xu, T. T. Han, Z. Q. Lu, W. Wang, J. Q. Peng, F. Du, F. L. Yang and X. Y. Ye, A Mn^{4+}-doped oxyfluoride phosphor with remarkable negative thermal quenching and high color stability for warm WLEDs, *Chem. Eng. J.* **392**, 123657 (2020).